Collective stacking faults and their effect on flux pinning in powder melting processed $Y_{0.6}Ho_{0.4}Ba_2Cu_3O_y$ superconductors

2000 J. Phys.: Condens. Matter 12 5843

(http://iopscience.iop.org/0953-8984/12/27/303)

J. Phys.: Condens. Matter **12** (2000) 5843–5855. Printed in the UK PII: S0953-8984(00)13137-6

Collective stacking faults and their effect on flux pinning in powder melting processed $Y_{0.6}Ho_{0.4}Ba_2Cu_3O_y$ superconductors

Y Feng†, J G Wen‡, A K Pradhan†, N Koshizuka† and L Zhou§

† Superconductivity Research Laboratory, ISTEC, 1-10-13 Shinonome, Koto-ku, Tokyo 135-0062, Japan

‡ Physics Department, Boston College, 140 Commonwealth Avenue, Chestnut Hill, MA 02167, USA

§ Northwest Institute for Nonferrous Metal Research, PO Box 51, Xi'an Shaanxi 710016, People's Republic of China

Received 7 April 2000, in final form 16 May 2000

Abstract. We have fabricated the highly textured $Y_{0.6}Ho_{0.4}Ba_2Cu_3O_y$ bulk superconductors by a powder melting process (PMP) method and investigated the microstructure and flux pinning characteristics. The microstructural observations show that there are many collective 'stair like' stacking faults in our sample, which is quite different from other melt-processed $YBa_2Cu_3O_y$. The formation of these stacking faults is discussed. It is found that the density of stacking faults is dramatically reduced when the sample is annealed at high temperature. After annealing, the critical current density and irreversibility line are significantly decreased in $H \parallel c$ and $H \parallel ab$ at various temperatures. These results clearly indicate that these stacking faults are very effective pinning centres in the PMP YBCO superconductors over a wide temperature and field range. The effect of stacking faults on the flux pining is sensitive to temperature and magnetic field. Also, the influences of stacking faults on the relaxation rate, the apparent pinning potential and the anisotropy of critical current are briefly studied.

1. Introduction

The exciting field for the applications of $YBa_2Cu_3O_y$ (123) superconductors is large scale power systems such as energy storage system, current limiters, magnetic bearings etc. For these applications, high critical current density (J_c) is required. Recently, melt processes such as melt textured growth (MTG) [1], melt–powder–melt growth (MPMG) [2], the liquid phase process [3] and the powder melting process (PMP) [4] are widely used to prepare 123 superconductors with high J_c exceeding 10^4 A cm^{-2} at 77 K. In addition, highly textured 123 samples have been fabricated by solidification in a magnetic field [5]. Although it is possible to obtain high quality 123 samples by using these methods, the flux creep and flux motion due to high operating temperature (77 K) make it difficult to maintain high J_c in the presence of magnetic fields. Therefore, the flux pining in melt-textured specimens should be improved to meet the requirements of the applications.

It is well known that the flux pinning is an extrinsic property related to the crystal defects and impurities in superconductors. Extensive microstructural investigations have shown that many defects such as oxygen deficiencies, stacking faults, twins, dislocations and columnar defects induced by ion irradiation are found in the melt-processed 123 samples. Some of

0953-8984/00/275843+13$30.00

them are proposed to be flux pinning candidates [6–11]. Also, it has been reported that even though the non-superconducting Y_2BaCuO_5 (211) particles are too big to be effective pinning centres, the superconducting and mechanical properties are enhanced by the introduction of 211 particles. The 123/211 interfaces or the defects associated with the interfaces are believed to be the flux pinning sites [12–14]. To date, the effectiveness of the possible pinning centres has not been fully understood although great progress has been made in increasing the flux pinning in the melt-textured 123 samples. Many studies were carried out to understand the formation mechanism and flux pinning role of stacking faults [15, 16]. It is reported that stacking faults were widely found in the melt-processed 123 samples and most of them consist of a double CuO chain. Some research indicated that these defects may act as effective pinning centres [17, 18], whereas it was also found that their contribution to the flux pinning may be detrimental under some conditions [19]. The previous work has shown that the flux pinning can be improved through the introduction of stacking faults created by the addition of CuO to Y123 and the shock-compacted process [20, 21]. However, their effectiveness in the flux pinning at different temperatures and fields has not been fully established and should be further investigated. In this paper, we fabricated $Y_{0.6}Ho_{0.4}Ba_2Cu_3O_y$ bulk superconductors by the PMP method and studied the microstructural features by transmission electron microscopy (TEM). The J_c values of the samples with different numbers of stacking faults have been analysed to reveal the effect of stacking faults on the flux pinning at various fields and temperatures.

2. Experiment

The sample with nominal compositions of $Y_{0.6}Ho_{0.4}Ba_2Cu_3O_y$ was prepared by the powder melting process technique. In the PMP method, the 211 and Ba–Cu–O phases were used as the precursors instead of the 123 phase commonly adopted in other melt processes. The precursor powders of $Y_{1.2}Ho_{0.8}BaCuO_5$ and $BaCuO_2$ were synthesized through a solid state reaction technique using Y_2O_3, Ho_2O_3, $BaCO_3$ and CuO. Then, these powders were well mixed in an appropriate ratio and were cold pressed into a rectangular shape. The bars were put into a tube furnace with the highest temperature of 1025 °C. The moving rate was about 3 mm h^{-1}. Finally, the sample was annealed at 550 °C for 40 h in flowing oxygen to insure complete oxygenation of the sample. Also, annealing was continued to 400 °C at a slow cooling rate of 3 °C h^{-1} for possible additional oxygen loading and to room temperature at 5 °C min^{-1}. This sample was labelled 'as melted'. Then, a small piece was cut off from the specimen for TEM observations. The sample for TEM observation was obtained by polishing to the thickness of 20 μm followed by Ar ion milling.

Critical temperature was measured by a superconducting quantum interference device (SQUID) magnetometer. Magnetization measurements were carried out using a SQUID magnetometer with the magnetic field parallel to and perpendicular to the c-axis of the sample at different temperatures. After these measurements, the same sample was annealed at 900 °C for 30 h to reduce the density of the stacking faults. Then, the sample (marked 'annealed') was subjected to the same oxygen treatment as the as-melt specimen. The magnetic hysteresis loops were again measured and the microstructure was observed by TEM.

3. Results and discussion

It is well established that the superconducting and physical properties of melt-processed YBCO samples are highly dependent on the microstructural features. The microstructure, however, is strongly related to the sample processing methods. Figure 1 gives a typical TEM photograph

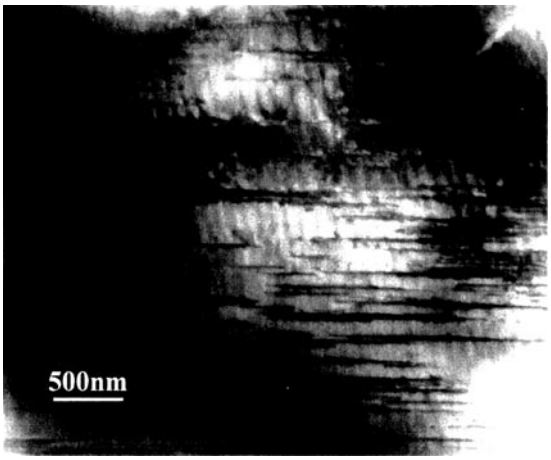

Figure 1. A typical TEM image of the as-melted sample displaying high density of stacking faults.

of the as-melted specimen. A high density of stacking faults parallel to the *ab*-plane is found in this sample. Extensive observations indicate that most stacking faults are collective and 'stair-like' as shown in figure 2, which is quite different from the stacking faults randomly observed in MTG and MPMG samples. Also, the density of stacking faults in our sample is much higher than that in other melt-processed YBCO. It is identified that the stacking fault in this sample is an excess CuO layer forming a local double chain layer, i.e. a local $YBa_2Cu_4O_y$ (Y124) phase. In addition, after checking several 211 particles, we found that the stacking faults are not related to the 211 particles. Figure 3 illustrates the TEM image of stacking faults in the specimen, showing no relation between stacking faults and 211 particles. This conclusion is not in agreement with other results [22], in which the authors reported that the density of stacking faults close to the 123/211 interfaces is much higher than that within the 123 matrix. On the other hand, Sandiumenge *et al* observed that the density of stacking faults increases dramatically at particular places. A high density of stacking faults is found in the 211 particle-free region. Also, there is no net increase of their density on increasing the density of the 211 particles [23]. These results support our observations that stacking faults are not related to the 211 particles.

The formation mechanism of the stacking faults has been investigated by many researchers [24, 25]. Although the origin of the stacking faults has not been clearly understood in the melt-processed YBCO, the stacking faults are considered to be formed during the solidification process. We think that the formation of stacking faults in our sample is due to a local CuO excess rather than the strain between 123 and 211. This CuO excess may be created by the non-equilibrium cooling and fast cooling in the PMP technique during the growth of the 123 material. Another possible mechanism is proposed to be related to the oxygen annealing process [26]. It is found that the Y123 phase is unstable at oxygen pressure values above 10^{-3} bar around 450 °C and the Y123 and Y124 transformation may occur in the oxygen annealing [27]. The following experiment rules out the possibility of such a mechanism in our sample.

In order to further investigate the flux pinning effect of stacking faults, the same specimen was annealed at 900 °C for 30 h followed by the same oxygen treatment as the as-melted sample. After this high temperature annealing, the microstructure of the sample has some changes. Figure 4 shows a TEM image of the annealed sample. It can be obviously seen

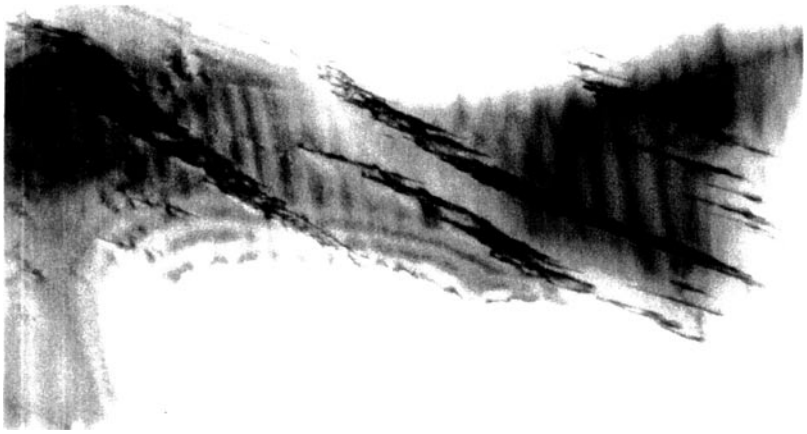

Figure 2. A TEM photograph of the as-melted specimen. Note that the stacking faults are collective and 'stair-like'.

Figure 3. A TEM image of the as-melted sample showing no relation between stacking faults and 211 particles.

that the density of stacking faults is dramatically reduced by this annealing. This is easily understood because the Y124 phase is unstable and will decompose to Y123 and CuO at high temperature [28]. If stacking faults are formed during the oxygenation process, their density in the annealed sample should be similar to that in the as-melted specimen since these two samples were subjected to the same oxygen treatment. However, their density is much decreased by the annealing treatment at 900 °C. Therefore, we believe that the formation of stacking faults in our sample may be related to the solidification process. Moreover, such a large substitution of Ho at the Y site may induce the formation of additional stacking faults.

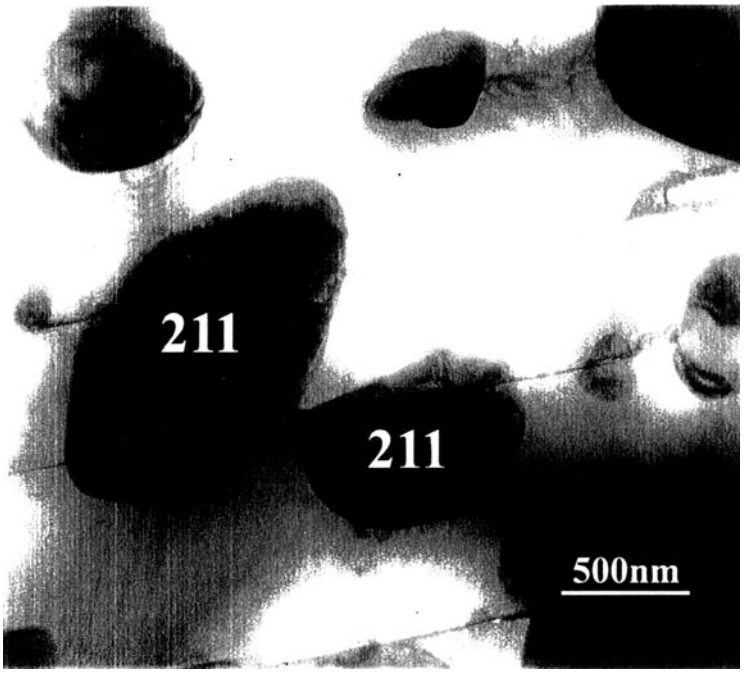

Figure 4. A TEM photograph of the annealed sample showing a huge reduction of the density of stacking faults.

In addition, extensive microstructural observations show that the plate 123 crystals are also highly textured with their *ab*-planes in the annealed sample. The size, number and distribution of the 211 particles in the annealed sample are almost the same as the as-melted specimen. Furthermore, twin boundaries in the annealed sample do not change after the high temperature annealing.

The critical temperatures of the as-melted and annealed samples were tested by a SQUID magnetometer with the magnetic field (10 Oe) parallel to the *c*-axis of the sample. The result indicates that T_c is about 91 and 90.8 K for the as-melted sample and annealed specimen, respectively. The transition width is around 0.8 K for the two samples, suggesting a homogenous oxygen distribution over the sample. This means that there is no change in T_c after the high temperature annealing process.

The critical current density of the samples both in H parallel to and perpendicular to the *c*-axis is estimated from the magnetization by using Bean's critical state model [29]. The magnetic field dependence of J_c for the as-melted and annealed samples at different temperatures is shown in figures 5 and 6. J_c in H parallel to the *c*-axis for the as-melted sample is quite high, about 7.6×10^4 A cm^{-2} at 77 K and 0.1 T, indicating that the flux pinning in this sample is very strong. It may be observed that J_c is severely reduced, to 2.2×10^4 A cm^{-2} at the same condition, for the annealed specimen. The result clearly suggests that the stacking faults are effective pinning centres in the low field region at high temperatures since only the density of stacking faults is remarkably decreased after the annealed process at 900 °C. This conclusion is different from other reports, in which the flux pinning at low fields in the 123 materials is believed to be associated with the 123/211 interfaces rather than stacking faults [30]. This divergence may originate from the different kind and density of sacking faults in other samples. In addition, it is also found in figures 5 and 6 that J_c is significantly reduced

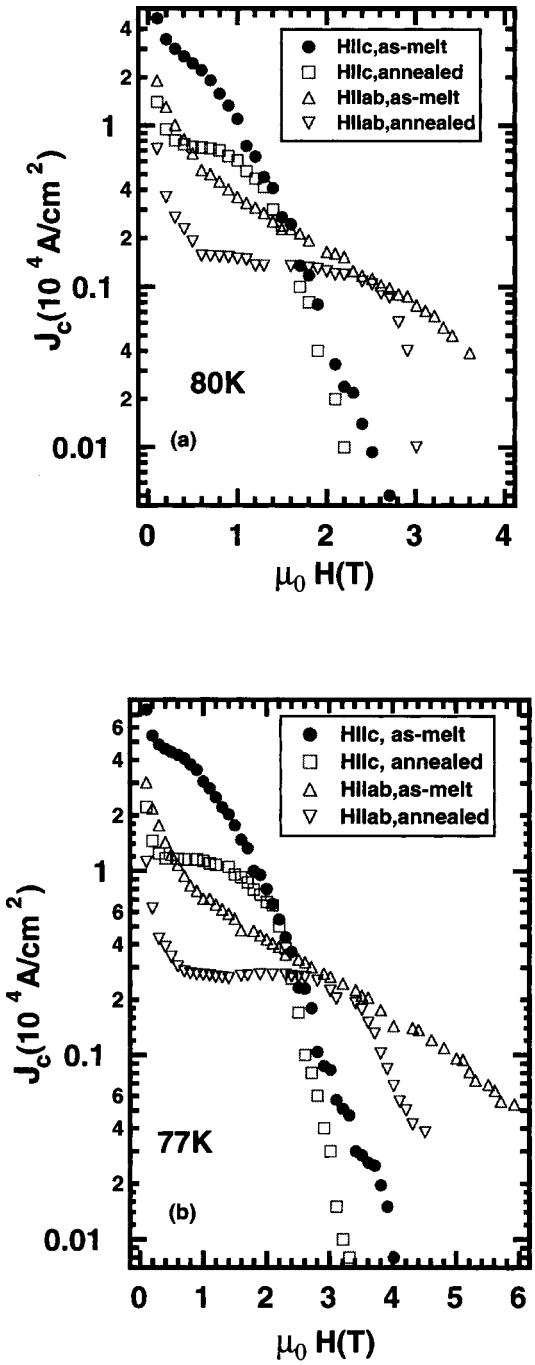

Figure 5. Critical current density as a function of magnetic field for the as-melted and annealed samples at (a) 80 K and (b) 77 K.

in the annealed sample at temperatures from 40 to 80 K in high and low fields for both field orientations. The decrease of J_c after the annealing process is not only temperature dependent

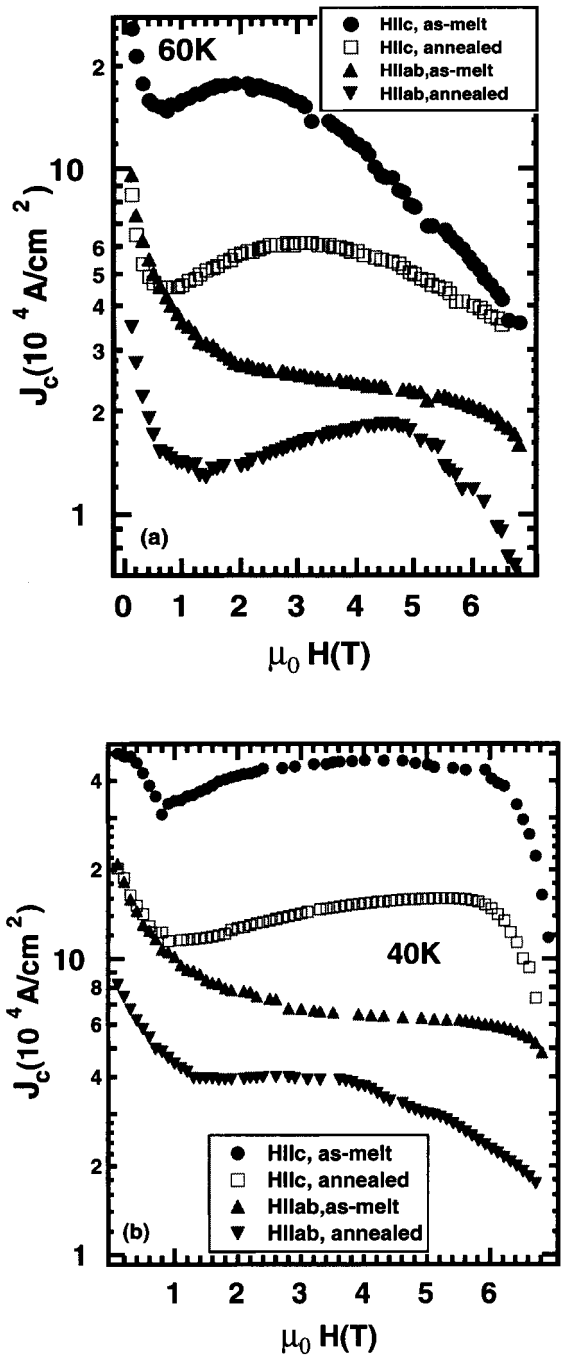

Figure 6. Critical current density versus magnetic field for the as-melted and annealed samples at (a) 60 K and (b) 40 K.

but also field dependent. The ratio (α) of J_c in the as-melted sample over J_c in the annealed specimen is calculated and the results are displayed in figure 7. It can be seen that this ratio is roughly the same for both field orientations at high temperatures, while it is larger in most

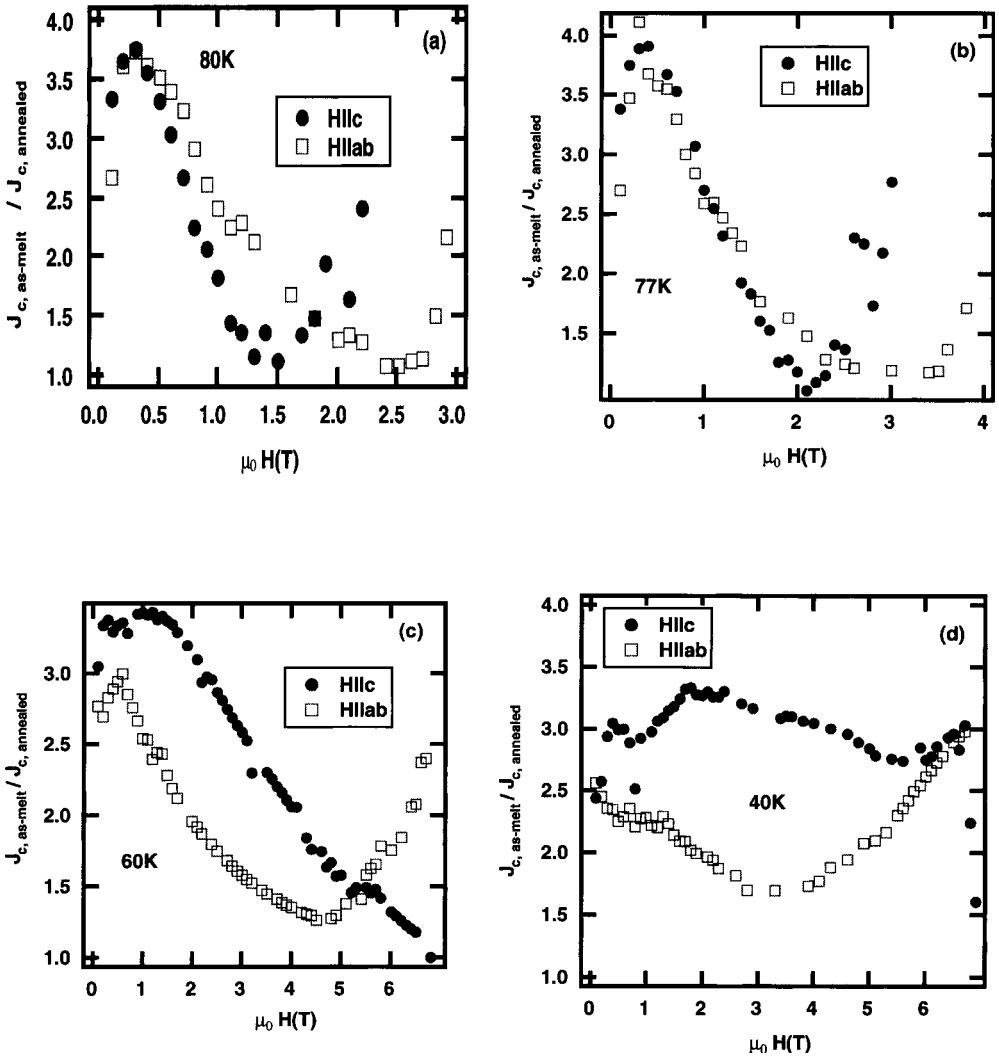

Figure 7. Field dependence of the ratio of J_c in the as-melted sample over J_c in the annealed specimen at (a) 80 K, (b) 77 K, (c) 60 K and (d) 40 K.

field regions for $H \parallel c$ than that for $H \parallel ab$ at low temperatures (60 and 40 K). Moreover, our data can be basically divided into three regions except for the data at 40 K: (1) α increases with initially increasing field and reaches its maximum; (2) α drops with the further increase of the field; (3) α rises again in high fields. It is interesting to note that the field corresponding to the maximum α remains around 0.4 T at these temperatures. At 77 and 80 K, the fact that α increases with the increase of the field in high fields can be explained as follows. The irreversibility line moves to low field after the annealing process as shown in figure 8. The irreversibility field is reduced from 3.4 T in the as-melted specimen to 2.4 T in the annealed sample at 80 K for $H \parallel c$. When the field approaches the irreversibility line J_c drops quickly. Therefore, J_c in the annealed sample decreases rapidly in the high fields near its irreversibility field, while J_c in the as-melted specimen falls off slowly in this field region compared to the annealed sample. This will result in the increase of α in high fields. In addition, the field at

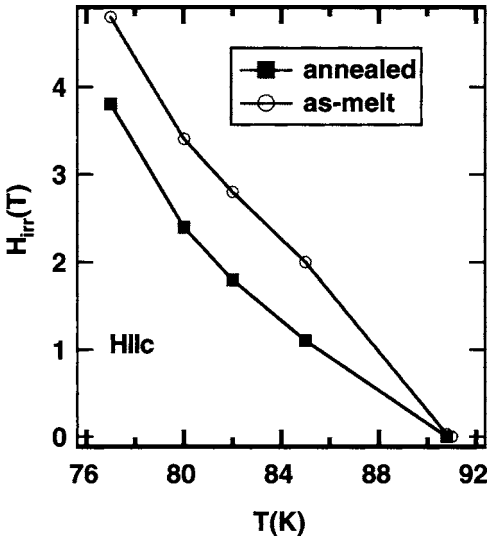

Figure 8. Irreversibility field with $H \parallel c$ versus temperature for the as-melted and annealed samples. The irreversibility line is remarkably decreased in the annealed sample.

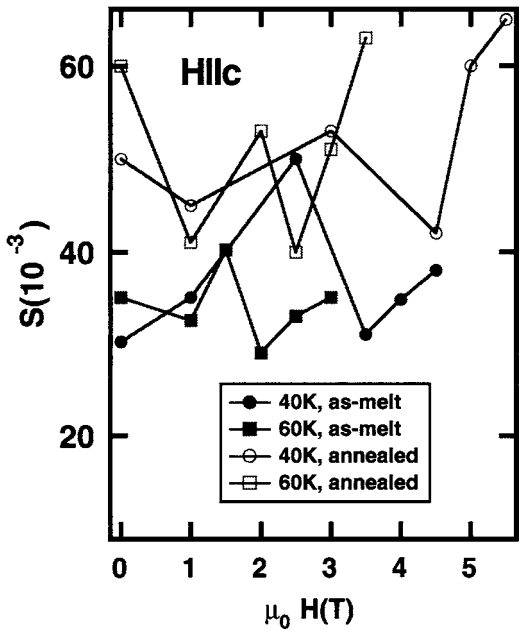

Figure 9. Field dependent normalized relaxation rate at 40 and 60 K in $H \parallel c$ for the two samples.

which α starts to rise shifts to higher field in $H \parallel ab$ than in $H \parallel c$ since the irreversibility field for $H \parallel ab$ is larger than that for $H \parallel c$ (as seen in figures 5(a) and (b)). However, for 60 K and $H \parallel ab$, α begins to increase at field away from the irreversibility line. This is because a peak effect is developed in the annealed sample for $H \parallel ab$ and no peak is observed in the as-melted sample (see figure 6(a)). It is noted that the absolute J_c value for $H \parallel ab$ in the annealed sample remains lower than that in the as-melted specimen. On the other hand, a

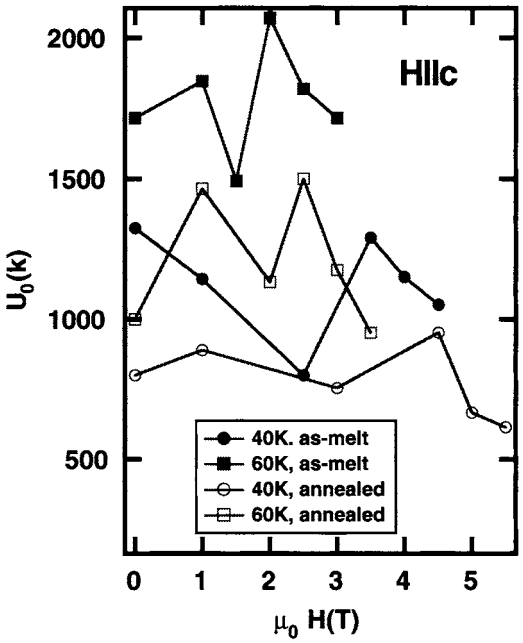

Figure 10. Field dependence of the apparent pinning potential with $H \parallel c$ at 40 and 60 K.

plateau feature in J_c is observed for $H \parallel ab$ at 40 K in the annealed sample. This behaviour in J_c of the annealed sample may be attributed to the random point defect pinning which becomes active when the correlated pinning behaviour of the stacking faults is removed on annealing. This feature is also noticed for $H \parallel c$ in the annealed sample at 60 K. The peak field is shifted to higher field values for $H \parallel ab$ as expected. At 40 K, α is about 3 for $H \parallel c$ from 1 to 6 T, which can be interpreted by the broad peak effect shown in figure 6(b).

From the above discussion we can conclude that these collective 'stairlike' stacking faults are very strong pinning centres in a wide range of temperatures and fields for both field orientations. The contribution of stacking faults to the flux pinning is temperature and field dependent. The effect of stacking faults on the flux pinning becomes larger with the initial increase of the field and achieves a maximum at low field. Then, their flux pining role is weaker in high fields but is also strong.

In order to obtain additional support in favour of the flux pinning effect of stacking faults, the time decay of the magnetization was measured in a zero-field cooled condition for 3600 s at 40 and 60 K in various fields for the as-melted and annealed samples. A magnetic field much higher than the field for full penetration was applied before each decay measurement to ensure the critical state. Figure 9 gives the field dependence of the normalized relaxation rate $S = -(\mathrm{d}M/\mathrm{d}\ln t)/M_0$ in $H \parallel c$, which was determined from the relaxation curves. It can be observed that the relaxation rate in the annealed sample is always larger than that in the as-melted specimen, indicating that the presence of stacking faults can reduce the flux creep. Also, an interesting feature in figure 9 is that a minimum value of S is found at each temperature in high field for the as-melted and annealed samples. For example, at 60 K the minimum in S occurs around 2 and 2.5 T for the as-melted sample and annealed specimen, respectively. It is expected that this minimum in the relaxation rate may be related to the fishtail effect since the flux pinning should be improved near the fishtail region. The field corresponding

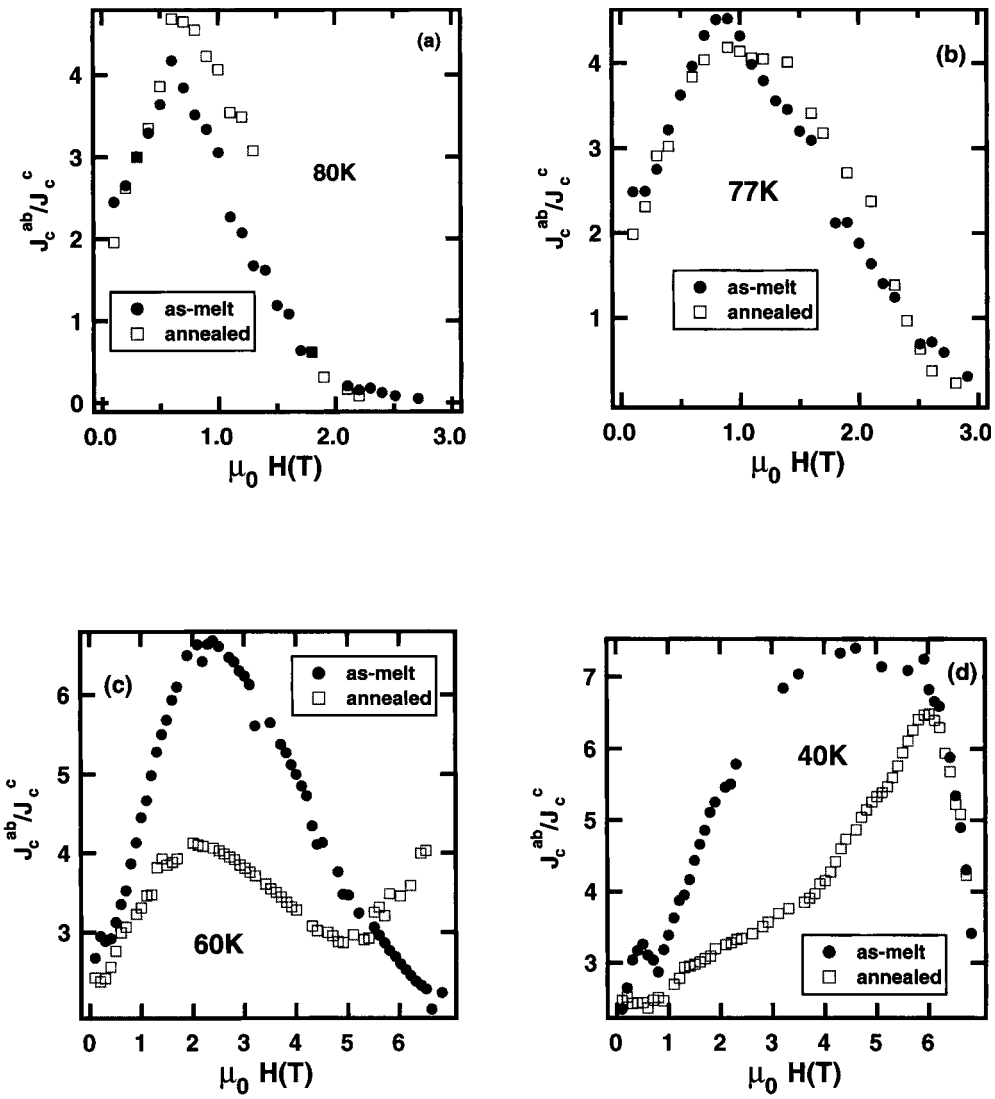

Figure 11. Anisotropy of critical current density (J_c^{ab}/J_c^c) as a function of magnetic field at (a) 80 K, (b) 77 K, (c) 60 K and (d) 40 K.

to the minimum S is lower than the field for the fishtail maximum (seen in figure 6(a) and (b)), which is agreement with another report [31]. On the other hand, the apparent pinning potential U_0 of the samples was estimated from the expression based on the Anderson–Kim model $U_0 = -kT/S$. In figure 10, we present U_0 as a function of the field at 40 and 60 K for the specimens in $H \parallel c$. As observed in this figure, the as-melted sample exhibits a higher value of the pinning potential at each temperature. This result clearly suggests that the pinning potential is also improved by the stacking faults.

Generally speaking, the anisotropy of critical current $\{J_c^{ab}(H \parallel c)/J_c^c(H \parallel ab)\}$ is related to the microstructural anisotropy of the linear and planar defects, the intrinsic anisotropy of vortices and the field dependence of J_c in both field orientations. Figure 11 shows the ratio

of J_c^{ab}/J_c^c versus field at various temperatures for the as-melted and annealed samples. The anisotropy increases with the decrease in temperature. At 40 K, the maximum ratio of J_c^{ab}/J_c^c for the as-melted sample is about 7.4, while the anisotropy in a YBCO single crystal is much higher, around 68 [32]. This result means that the flux pinning mechanism in a single crystal is totally different from that in our sample. From figure 11, it can be observed that there is a maximum value in the anisotropy of critical current at each temperature for the as-melted and annealed samples. Also, the field for this maximum shifts toward higher field as temperature drops. The ratios of the annealed sample at 77 and 80 K are similar to those of the as-melted specimen, whereas the anisotropy in the annealed sample is much lower than that in the as-melted sample for 40 and 60 K. This result implies that the stacking faults in our sample have a big influence on the anisotropy of critical current at low temperatures. The reduction of stacking faults will lead to a decrease in the anisotropy at low temperatures.

4. Conclusion

We have investigated the microstructural features and flux pinning of $Y_{0.6}Ho_{0.4}Ba_2Cu_3O_y$ bulk superconductors fabricated by a PMP method. A high density of collective 'stair-like' stacking faults is observed in the sample. These stacking faults are believed to be probably formed during the solidification process, which is correlated to the characteristics of the PMP technique. A high temperature annealing process will result in a huge elimination of stacking faults and a significant decrease of J_c for both field directions at various temperatures. The relaxation result also indicates that the presence of stacking faults can severely suppress the flux creep and improve the apparent pinning potential. It is concluded that these stacking faults can act as strong pinning centres in PMP 123 superconductors in a wide range of temperatures and fields in both field orientations. Their contribution to the flux pinning is not only field dependent but also temperature dependent. These stacking faults have a largest effect on the flux pinning in low fields. Moreover, the anisotropy of critical current is decreased by the reduction of the density of stacking faults at low temperatures.

Acknowledgments

This work is supported by the New Energy and Industrial Technology Development Organization (NEDO) as Collaborative Research and Development of Fundamental Technologies for Superconductivity Applications.

References

[1] Jin S, Tiefei T H, Sherwood R C, Davis M E, van Dover R B, Kammlott G W, Fastnacht R A and Keith H D 1988 *Appl. Phys.* **53** 2074
[2] Salama K, Selvamanickam V, Gao L and Sun K 1989 *Appl. Phys. Lett.* **54** 2352
[3] Murakami M, Morita M, Doi K and Migyamoin 1989 *Japan. J. Appl. Phys.* **28** 1189
[4] Zhou L, Zhang P, Ji P, Wang J, Wang K and Wu X 1990 *Supercond. Sci. Technol.* **3** 390
[5] Bourhault D, de Rengo P, Barbut T M, Braithwaite D, Lees M R, Peijay P, Sulpice A and Tournier R 1992 *Physica* C **194** 177
[6] Kes P H 1991 *Physica* C **185–9** 288
[7] Chudnovsy E M 1990 *Phys. Rev. Lett.* **65** 3060
[8] Ekin J W, Salama K and Selvamanickam V 1991 *Appl. Phys. Lett.* **59** 360
[9] Lee D F, Salama K, Selvamanickam V and Forster K 1992 *Physica* C **202** 83
[10] Daemuling M, Seuntjiens J M and Larbalestier D C 1990 *Nature* **346** 332
[11] Zhang Y, Mironva M, Lee D F and Salama K 1993 *Japan. J. Appl. Phys.* **34** 3077

[12] Murakami M, Gotoh S, Fujimoto H, Yamaguchi K, Koshizuka N and Tanaka S 1991 *Supercond. Sci. Technol.* **4** S93
[13] Muralami M, Gotoh S, Fujimoto H, Yamaguchi K, Koshizuka N and Tanaka S *Physica* C **185–9** 321
[14] Lee D L, Chaud Z and Salama K 1993 *Interface Sci.* **11** 385
[15] Zanota A, Kvam E P, Balkin D and McGinn D J 1993 *Appl. Phys. Lett.* **62** 2722
[16] Puig T, Plain J, Sandiumenge F, Obradors X, Rabier J and Alonso J A 1999 *Appl. Phys. Lett.* **75** 1952
[17] Zhang P X, Zhou L, Ji P, Bian W M, Wu X Z and Lai Z H 1995 *Supercond. Sci. Technol.* **8** 15
[18] Martinez B, Sandiumenge F, Puig T, Obradors X, Richard L and Rabier J 1999 *Appl. Phys. Lett.* **74** 72
[19] Obradors X, Yu R, Sandiumenge F, Martinez B, Vilata N, Gomis V, Puig T and Pinol S 1997 *Supercond. Sci. Technol.* **10** 884
[20] Kramer M J 1991 *Appl. Phys. Lett.* **58** 1086
[21] Wier S T, Nellis W T, Kramer M J, Early E A, Seaman C L and Maple M B 1990 *Appl. Phys. Lett.* **59** 2042
[22] Wang Z L, Goyal A and Kroeger D M 1993 *Phys. Rev.* B **47** 5373
[23] Sandiumenge F, Pinol S, Obradors X, Snoeck E and Roucau C 1994 *Phys. Rev.* B **50** 7032
[24] Wang R K, Ren H T, Xiao L, He Q and Yu D 1990 *Supercond. Sci. Technol.* **3** 344
[25] Vilata N, Sandiumenge F, Rogriguez E, Martinez B, Pinol S, Obradors X and Rabier J 1997 *Phil. Mag.* B **75** 431
[26] Kim C J, Kim K B, Park H W, Sung T H, Kuk I H and Hong G W 1996 *Supercond. Sci. Technol.* **9** 76
[27] Morris D, Markolz A G, Fayss B and Nizkel J H 1990 *Physica* C **168** 153
[28] Shrivastava A K, Chandrashekhar T V and Shrivastava O N 1994 *Supercond. Sci. Technol.* **7** 551
[29] Bean C P 1964 *Rev. Mod. Phys.* **36** 31
[30] Martinez B, Obradors X, Gou A, Gomis V, Pinol S, Fatcuberta J and Van Tol H 1996 *Phys. Rev.* B **53** 2797
[31] Jirsa M, Pust L and Koblishika M R 1997 *Phys. Rev.* B **55** 3276
[32] Schomman K, Seebacker B and Andres F 1991 *Physica* C **184** 47